

Plasmonic nano-patch array with integrated metal-organic framework for enhanced infrared absorption gas sensing

This content has been downloaded from IOPscience. Please scroll down to see the full text.

Download details:

IP Address: 132.174.255.116

This content was downloaded on 26/05/2017 at 15:25

Manuscript version: Accepted Manuscript

Chong et al

To cite this article before publication: Chong et al, 2017, Nanotechnology, at press:

<https://doi.org/10.1088/1361-6528/aa7433>

This Accepted Manuscript is: © 2017 IOP Publishing Ltd

During the embargo period (the 12 month period from the publication of the Version of Record of this article), the Accepted Manuscript is fully protected by copyright and cannot be reused or reposted elsewhere.

As the Version of Record of this article is going to be / has been published on a subscription basis, this Accepted Manuscript is available for reuse under a CC BY-NC-ND 3.0 licence after the 12 month embargo period.

After the embargo period, everyone is permitted to copy and redistribute this article for non-commercial purposes only, provided that they adhere to all the terms of the licence

<https://creativecommons.org/licenses/by-nc-nd/3.0>

Although reasonable endeavours have been taken to obtain all necessary permissions from third parties to include their copyrighted content within this article, their full citation and copyright line may not be present in this Accepted Manuscript version. Before using any content from this article, please refer to the Version of Record on IOPscience once published for full citation and copyright details, as permission will likely be required. All third party content is fully copyright protected, unless specifically stated otherwise in the figure caption in the Version of Record.

When available, you can view the Version of Record for this article at:

<http://iopscience.iop.org/article/10.1088/1361-6528/aa7433>

1 2 Plasmonic nano-patch array with integrated metal-organic 3 framework for enhanced infrared absorption gas sensing 4 5

6 Xinyuan Chong,¹ Ki-joong Kim,^{2,3,5} Yujing Zhang,² Erwen Li,¹ Paul R. Ohodnicki,^{3,4} Chih-Hung Chang² and Alan X. Wang^{1,*}
7

8 ¹ School of Electrical Engineering and Computer Science, Oregon State University, Corvallis, OR 97331, USA
9

² School of Chemical, Biological and Environmental Engineering, Oregon State University, Corvallis, OR 97331, USA
10

³ National Energy Technology Laboratory (NETL), U.S. Department of Energy, 626 Cochran's Mill Road, Pittsburgh, PA 15236, USA
11

⁴ Materials Science and Engineering, Department, Carnegie Mellon University, Pittsburgh, PA 15213, USA
12

⁵ AECOM, 626 Cochran's Mill Road, Pittsburgh, PA 15236, USA
13

*Corresponding author: wang@eecs.oregonstate.edu
14

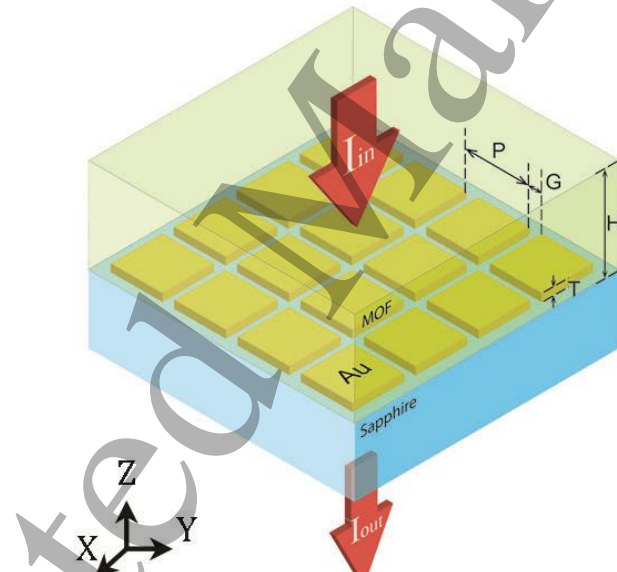
15 **Abstract:** In this letter, we present a nanophotonic device consisting of plasmonic nano-patch array with integrated
16 metal-organic framework (MOF) for enhanced infrared absorption gas sensing. By designing a gold nanopatch
17 array (Au-NPA) on a sapphire substrate, we are able to achieve enhanced optical field that spatially overlaps with
18 the MOF layer, which can adsorb carbon dioxide (CO₂) with high capacity. Experimental results show that this
19 hybrid plasmonic-MOF device can effectively increase the infrared absorption path of on-chip gas sensors by more
20 than 1,100-fold. The demonstration of infrared absorption spectroscopy of CO₂ using the hybrid plasmonic-MOF
21 device proves a promising strategy for future on-chip gas sensing with ultra-compact size.
22
23

24 25 Introduction 26

27 Metal-organic frameworks (MOFs), a new class of nanoporous materials, have attracted intensive research
28 interests due to their large surface area and wide structure tunability. MOFs are extended crystalline structures
29 consisting of metal ions connected by organic ligands, which can essentially possess an infinite number of possible
30 combinations with different physical and chemical properties. Therefore, MOFs have been widely applied in
31 chemical separation[1], gas storage[2-5], drug delivery[6], sensing[7-10], and catalysis[11-14] applications. In
32 recent years, hybrid plasmonic-MOF nanostructures have been reported to take the advantages of the strong gas
33 adsorption capabilities of MOF materials and the optical field enhancement of plasmonics effect. These hybrid
34 nanostructures have been applied in different applications, such as catalysis[15-18], imaging[19], surface-enhanced
35 Raman scattering (SERS)[20-27] and surface-enhanced infrared absorption (SEIRA)[9]. However, most of these
36 reported hybrid plasmonic-MOF nanostructures are based on chemically synthesized metallic or semiconductor
37 nanoparticles, which have several drawbacks. First, the optical field enhancement of plasmonic NPs comes from the
38 intrinsic plasmonic resonance of free electrons, which has strong optical scattering and relatively low Quality-
39 factors (Q-factors) of only about 4~5. Considering a large amount of randomly distributed plasmonic NPs, the
40 optical transmission through the thin film is relatively low. Second, the enhanced optical field from intrinsic
41 plasmonics effect of NPs are highly localized, mostly confined at the surface or between the NPs. This means that
42 the hot spot volume is very limited. Only the analyte molecules within the hot spot can interact with the highly
43 localized optical field. For example, in our previous work[9], the volume ratio of the hot spots in the hybrid indium-
44 tin oxide (ITO) NPs with Cu-BTC (BTC=benzene-1,3,5- tricarboxylate) MOF to enhance gas absorption is only
45 0.12% based on our numerical calculation. Therefore, the overall plasmonic field enhancement is only about 2.6
46 times from our numerical calculation. Last, the intrinsic plasmonic resonance of chemically synthesized NPs is
47
48
49
50
51
52
53
54
55
56
57
58
59
60

1 affected by free electron concentration, composition, size, geometry, and even the coupling between the NPs, which
 2 is difficult to control. Many experimentally results actually show much broader plasmonic resonances than
 3 simulation due to the inherent limitations and variation of fabrication process.

4 In this paper, we present a nanophotonic device consisting of a periodic plasmonic nano-patch array (NPA)[28]
 5 with integrated MOF layer to resolve the engineering challenges. Compared with randomly distributed plasmonic
 6 NPs relying on the intrinsic plasmonics effect[9] or triangular dipole nano-antennas with MOF [29], our design
 7 offers much higher Q-factors with higher optical transmission efficiency due to the constructive interaction of the
 8 surface plasmon polaritons (SPPs) at the interface between Au NPA and MOF thin film [30]. The optical field at the
 9 surface of the plasmonic NPA extends to the entire MOF layer, which can effectively increase the strength of light-
 10 matter interaction. In other words, more analyte molecules can be adsorbed and concentrated inside the MOF film
 11 and interact with the plasmonic field, which is crucial for enhanced infrared absorption. Moreover, the plasmonic
 12 resonance can be fine-tuned by the periodicity of the NPA, which can be precisely controlled by top-down
 13 lithography process. The large and precision tunability of plasmonic resonances offers the possibility to enhance the
 14 vibrational spectra sensing of various analytes and even for multiplexed sensing with high throughput.



43 Fig. 1. Schematic of the MOF integrated plasmonic nanopatch array. For geometrical parameters, P is the gold nanopatch period, G is the nano-slit width, H is
 44 the MOF thickness and T is the gold thickness. I_{in} and I_{out} stand for the intensity of the incident and transmitted light.

45 The device consists of a gold Au-NPA on a sapphire ($n_{\text{sapphire}} = 1.721$) substrate, which is covered by a thin
 46 layer of MOF ($n_{\text{MOF}} = 1.326$), zeolitic imidazolate frameworks (ZIFs) or ZIF-8, as shown in Figure 1. Light is
 47 launched from the MOF side, and the transmitted light is collected from the substrate. When the light is coupled
 48 into the device normal to the surface, surface plasmon resonances (SPRs) are excited at the Au/MOF interface and
 49 coupled with the Fabry-Pérot (FP) modes in the MOF layer as well. Since the Au-NPA is symmetric, the device is
 50 polarization independent. Based on the design, the parameters that can be modified are the periodicity (P) of the Au-
 51 NPA, gap width (G) between Au-NPs, the thickness (H) of the MOF layer and the Au thickness (T). In order to
 52 achieve high optical field enhancement within the MOF layer, optimization is performed by the DiffractMOD of
 53
 54
 55
 56
 57
 58
 59
 60

Rsoft photonic component design suite, which is based on rigorous coupled-wave analysis (RCWA)[31]. Among these parameters, the MOF thickness (H) is the most important one. The optical effect of the parameters is well-studied in the literature for plasmonic nano-antennas[32]. The periodicity (P) of the Au-NPA determines the peak wavelength; the gap (G) affects the transmission intensity and also the spectrum width; the Au thickness (T) also has an influence on the transmission intensity. In this paper, we focused on the detailed study of the MOF thickness (H) as it not only affects the optical field enhancement, but also determines the infrared absorption path.

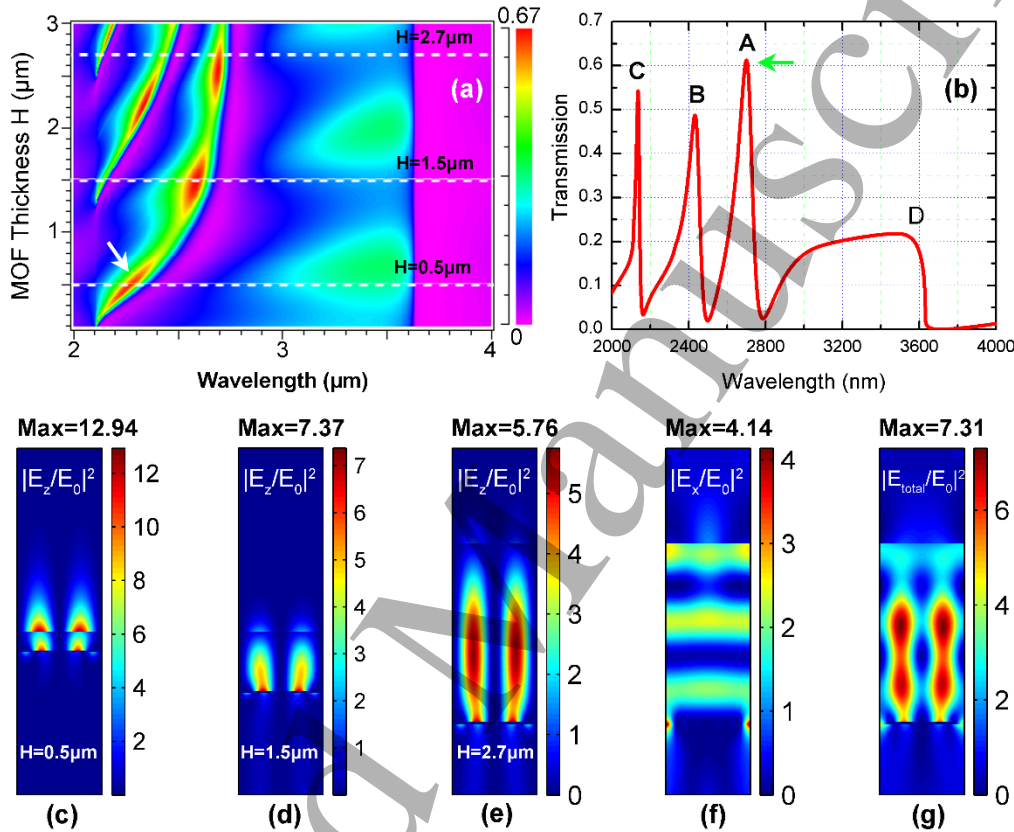


Fig. 2. (a) Effect of the MOF thickness H in transmission intensity, with fixed P, T and G. The color bar represents the transmission intensity. (b) Simulated transmission spectrum for H = 2.7 μ m. Electric distribution of z direction for (c) H = 0.5 μ m, (d) H = 1.5 μ m and (e) H = 2.7 μ m. (f) The electric field distribution of (f) x direction, and (g) the summation of all directions for H = 2.7 μ m.

A scanning of the MOF thickness (H) is performed by fixing other parameters. The transmission intensity results are shown in Figure 2(a). The major peak (indicated by the white arrow) shows a red-shift when the MOF thickness (H) increases from 0.4 μ m to 3.0 μ m. For real applications, the transmission intensity should be high enough to obtain good signal-to-noise ratio. Thus, the three peaks in the simulated transmission spectrum for H=2.7 μ m shown in Figure 2 (b) with over 50% transmission efficiency provide excellent measurement condition. In order to verify whether the thickness (H) is appropriate, three different values are selected from the three regions represented by the white dash lines. The electric field distributions of the three values of thickness at peak at 2.7 μ m after modifying the period are shown in Figure 2 (c-e). For H = 0.5 μ m, it has the highest field intensity, but most of the enhanced field is in air instead of in the MOF layer, which is not preferred by gas sensing. For H = 1.5 and 2.7 μ m, most of the field is confined in the MOF layer. If we only consider the plasmonic field, then H = 1.5 μ m is better than H = 2.7 μ m. However, we need to consider the amount of adsorbed gas by MOF in our design. In other

words, a thinner MOF layer means less gas molecules are adsorbed. Therefore, the relatively thicker MOF is more desirable to allow more gas molecules to interact with the optical field. Finally, after comprehensive consideration of the plasmonic effect, MOF's adsorbing property, transmission intensity and also growth time for the MOF layer, the parameters are determined to be $P = 2.11 \mu\text{m}$, $G = 250 \text{ nm}$, $H = 2.7 \mu\text{m}$, and $T = 40 \text{ nm}$. The simulated transmission spectrum is shown in Figure 2(e), which has three resonant peaks in the shorter wavelength range and one sharp edge at the longer wavelength. Peak A is the desired coupled mode with $\sim 60\%$ transmission efficiency with a relatively higher Q-factor of 27.44. The electric field distributions at peak A are shown in Figure 2(e) (E_z only, corresponding to the plasmonic resonance of the Au NPA), Figure 2(f) (E_x only, corresponding to the F-P resonance in the MOF thin film) and Figure 2(g) (total hybridized electric field). The maximum intensity enhancement is 7.31. Essentially, the coupled mode extends the highly localized plasmonic field to the entire MOF layer, resulting in an increase of the interaction between gas molecules inside the MOF and the optical field. Peak B and C are the higher modes of peak A, and the sharp edge D represents the Rayleigh anomaly at the substrate side[33].

Experiments and Results

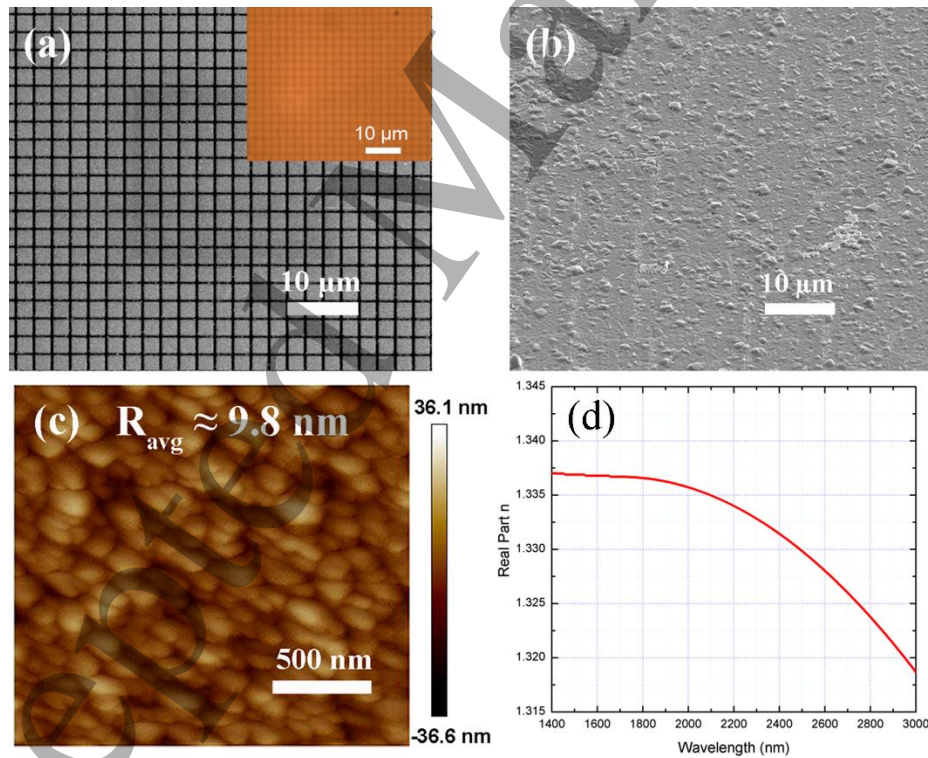


Fig. 3. (a) SEM image of fabricated Au- NPA. The inset is the optical image of the Au-NPA. (b) The SEM image of Au-NPA after growing MOF. (c) AFM image of the ZIF-8 thin film. (d) The refractive index of the MOF thin film.

The device is fabricated by focused ion beam (FIB) etching followed by monolithic growth of a MOF thin film. The selected MOF is the zeolitic imidazolate framework-8 (ZIF-8s), which has been extensively investigated due to its excellent thermal stability and selectivity toward CO_2 [34]. Besides, due to the hydrophobic surface property, water molecules can only be adsorbed at the outer surface, while CO_2 can diffuse into the inner pores.

Besides, the hydrophobic surface makes ZIF-8 even more attractive for chemical sensing in environments where water vapors are pervasive[34]. The growth process is described here briefly. Before growing the ZIF-8 film, the substrate with Au-NPA is cleaned in piranha solution ($\text{H}_2\text{SO}_4/\text{H}_2\text{O}_2$, 70/30 v/v%) at 70 °C for 30 minute. Then it is washed thoroughly by deionized water and dried under nitrogen flow. To grow ZIF-8 thin film, the cleaned Au-NPA sample is immersed in a freshly mixed methanolic solution of 2-methylimidazole and $\text{Zn}(\text{NO}_3)_2$ for 30 min at room temperature, followed by washing using methanol and drying under nitrogen flow. To obtain 2.7 μm MOF layer, this process is repeated 32 cycles. The scanning electron microscope (SEM) images of the fabricated Au-NPA before and after growing MOF are shown in Figure 3(a) and 3(b), respectively. As we can see, the MOF layer fully covers the Au-NPA and the MOF forms a relative smooth thin film with surface roughness about 10 nm, which is measured by atomic force microscopy (AFM) as shown in Figure 3 (c). The refractive index of the MOF thin film coated on a silicon wafer was measured by ellipsometry as shown in Figure 3(d).

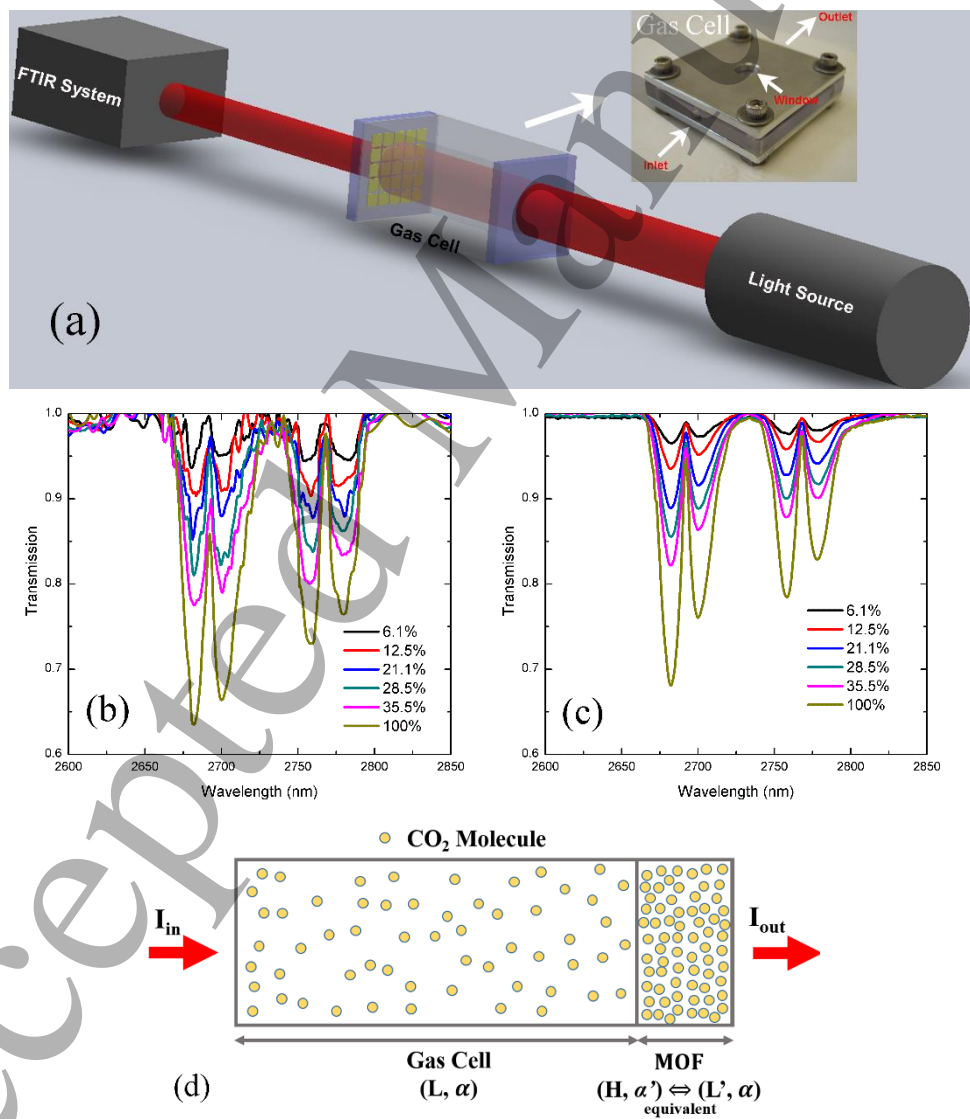


Fig.4. (a) Schematic of the experimental setup for gas sensing. Experimentally obtained transmission spectra of CO_2 for (b) Au-NPA coated with MOF at different CO_2 concentrations and (c) the reference. (d) Illustration of data analysis.

In order to quantitatively determine the enhancement provided by the hybrid plasmonic-MOF device, a CO₂ sensing measurement was performed by a Fourier transform infrared (FTIR) spectrometer system shown in Figure 4(a). The gas cell used in the system is home built with 4 mm light path length. One side of the gas cell is sealed by a sapphire window and the other side is sealed by the device. Different CO₂ concentrations are obtained by mixing with nitrogen (N₂) using two mass flow controllers. Figure 4(b) shows the transmission spectra of different CO₂ concentration. As a reference, the hybrid plasmonic-MOF device is replaced by bare sapphire window. As a comparison, the transmission spectra of the reference without any device are shown in Figure 4(c). The spectra in the manuscript have already been excluded from the effect of the plasmonic structure itself. Before taking the spectra of with CO₂, we measured the spectra of the device purged by Ar as reference. Since Ar molecules have no IR absorption around 2.7 μ m, the reference spectra only contain the IR spectra of plasmonic structure. Then, the measured spectra of the device with CO₂ were normalized to the reference spectra. Therefore, the spectra in the manuscript only account the IR absorption from CO₂. In order to determine the enhancement provided by the device, an analysis was performed as illustrated in Figure 4(d). Since the reference does not have any enhancement, the absorption is purely due to the CO₂ inside the gas cell. According to the Beer-Lambert law, the absorption coefficient α of the CO₂ inside the gas cell without the hybrid plasmonic-MOF device can be calculated using the following equation:

$$I_{\text{out}} / I_{\text{in}} = \exp(-\alpha \cdot L) \quad (1)$$

where L is the path length of the gas cell. For the gas cell with the hybrid plasmonic-MOF device, besides the CO₂ absorption in the gas cell, there is extra IR absorption from CO₂ molecules adsorbed inside the MOF. Therefore, the total IR absorption can be expressed as:

$$I_{\text{out}} / I_{\text{in}} = \exp(-\alpha \cdot L - \alpha' \cdot H) \quad (2)$$

where α' is the enhanced IR absorption coefficient of the CO₂ adsorbed inside MOF layer, which is larger than α . Since the IR absorption is only exponentially proportional to the product of absorption coefficient and optical path length, Equation (2) can be rewritten as Equation (3):

$$I_{\text{out}} / I_{\text{in}} = \exp(-\alpha \cdot L - \alpha \cdot L') \quad (3)$$

In Equation (3), L' is the equivalent optical path length provided by the plasmonic-MOF device, which has a physical length of H . Therefore, the enhancement factor (EF) is defined as $EF = L' / H$. The EF includes both the plasmonic field enhancement effect and also the gas concentrating effect from the MOF film. The calculated EF as a function of CO₂ is shown in Figure 5 using the experimental data in Figure 4, with the highest EF over 1,100. The nonlinear trend is due to the nonlinear absorption behavior of MOF, which is possibly due the different adsorption mechanism at high and low CO₂ concentration as we discussed in Reference [4]. At high concentration, most of the gas molecules are physically adsorbed inside the MOF pores, which are limited by the available space.

1 While at low concentration CO_2 , chemical bond adsorption becomes dominant [7, 8], which can provide a large
2 gas concentration factor.
3
4
5
6
7
8
9
10
11
12
13
14
15
16
17
18
19
20
21
22
23
24
25

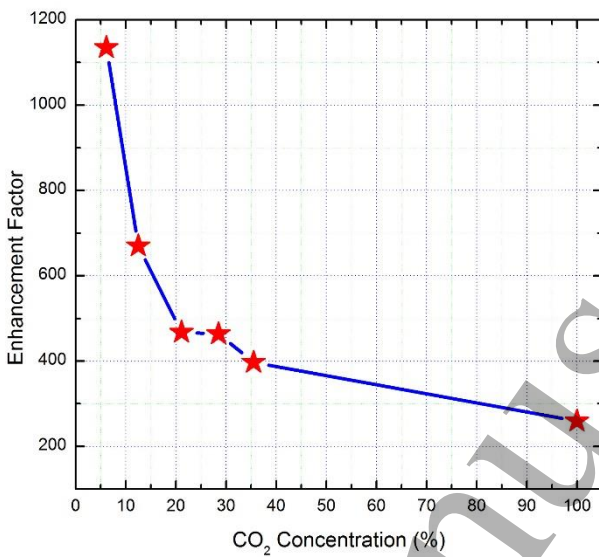


Fig.5. Enhancement factor of Au-NPA coated with MOF as a function of CO_2 concentration.

26 In summary, we present a hybrid plasmonic-MOF device by integrating plasmonic NPA with nano-porous
27 ZIF-8 MOF thin film. Compared with plasmonic NPs-enhanced MOF film, this new type of rationally designed
28 nanophotonic devices provide enhanced optical transmission, higher Q-factors, stronger light-matter interaction, and
29 tunable plasmonic resonances to match the vibrational spectra of the analytes. In this work, the hybrid plasmonic
30 NPA-MOF thin film device was integrated with a gas cell for CO_2 sensing at $2.7 \mu\text{m}$ wavelength. Based on Beer-
31 Lambert law, the total enhancement factor was calculated according to the experimental results. The highest EF
32 obtained is about 1,100. This device can be applied for on-chip IR gas sensing, which can potentially reduce the
33 absorption length of conventional gas cells by several orders of magnitude.
34
35
36
37
38
39
40
41
42
43
44
45
46
47
48
49
50
51
52
53
54
55
56
57
58
59
60

This technical effort was sponsored by the National Science Foundation under Grant No. 1449383. Xinyuan Chong and Yujing Zhang were partially supported by the Graduate Student Fellowship from the National Energy Technology Laboratory (NETL).

References

- [1] Sneddon G, Greenaway A and Yiu H H P 2014 The Potential Applications of Nanoporous Materials for the Adsorption, Separation, and Catalytic Conversion of Carbon Dioxide *Adv Energy Mater* **4** 1301873
- [2] Li L J, Tang S F, Wang C, Lv X X, Jiang M, Wu H Z and Zhao X B 2014 High gas storage capacities and stepwise adsorption in a UiO type metal-organic framework incorporating Lewis basic bipyridyl sites *Chem Commun* **50** 2304-7
- [3] Tylianakis E, Klontzas E and Froudakis G E 2009 The effect of structural and energetic parameters of MOFs and COFs towards the improvement of their hydrogen storage properties *Nanotechnology* **20** 204030
- [4] Brown C M, Liu Y, Yildirim T, Peterson V K and Kepert C J 2009 Hydrogen adsorption in HKUST-1: a combined inelastic neutron scattering and first-principles study *Nanotechnology* **20** 204025

1 [5] Li Q and Thonhauser T 2012 A theoretical study of the hydrogen-storage potential of (H-2)(4)CH₄ in metal
2 organic framework materials and carbon nanotubes *J Phys-Condens Mat* **24** 424204
3 [6] Levine D J, Runczewski T, Kapelewski M T, Keitz B K, Oktawiec J, Reed D A, Mason J A, Jiang H Z H, Colwell K
4 A, Legendre C M, FitzGerald S A and Long J R 2016 Olsalaiine-Based Metal-Organic Frameworks as
5 Biocompatible Platforms for H₂ Adsorption and Drug Delivery *J Am Chem Soc* **138** 10143-50
6 [7] Chong X, Kim K-J, Li E, Zhang Y, Ohodnicki P R, Chang C-H and Wang A X 2016 Near-infrared absorption gas
7 sensing with metal-organic framework on optical fibers *Sensors and Actuators B: Chemical* **232** 43-51
8 [8] Chong X Y, Kim K J, Ohodnicki P R, Li E W, Chang C H and Wang A X 2015 Ultrashort Near-Infrared Fiber-
9 Optic Sensors for Carbon Dioxide Detection *IEEE Sens J* **15** 5327-32
10 [9] Kim K J, Chong X Y, Kreider P B, Ma G H, Ohodnicki P R, Baltrus J P, Wang A X and Chang C H 2015
11 Plasmonics-enhanced metal-organic framework nanoporous films for highly sensitive near-infrared
12 absorption *J Mater Chem C* **3** 2763-7
13 [10] Hu Z H, Tao C A, Wang F, Zou X R and Wang J F 2015 Flexible metal-organic framework-based one-
14 dimensional photonic crystals *J Mater Chem C* **3** 211-6
15 [11] Wu C D and Lin W B 2007 Heterogeneous asymmetric catalysis with homochiral metal-organic
16 frameworks: Network-structure-dependent catalytic activity *Angew Chem Int Edit* **46** 1075-8
17 [12] Ma L Q, Falkowski J M, Abney C and Lin W B 2010 A series of isoreticular chiral metal-organic frameworks
18 as a tunable platform for asymmetric catalysis *Nat Chem* **2** 838-46
19 [13] Cao H, Zhu S Q, Yang C, Bao R Q, Tong L N, Hou L R, Zhang X G and Yuan C Z 2016 Metal-organic-
20 framework-derived two-dimensional ultrathin mesoporous hetero-ZnFe₂O₄/ZnO nanosheets with
21 enhanced lithium storage properties for Li-ion batteries *Nanotechnology* **27** 465402
22 [14] Hyeonseok Y, Alexander W, Wei G, Jinsub C and Engelbert R 2017 Electrodeposition of WO₃ nanoparticles
23 into surface mounted metal-organic framework HKUST-1 thin films *Nanotechnology* **28** 115605
24 [15] Tilgner D and Kempe R 2017 A Plasmonic Colloidal Photocatalyst Composed of a Metal-Organic
25 Framework Core and a Gold/Anatase Shell for Visible-Light-Driven Wastewater Purification from
26 Antibiotics and Hydrogen Evolution *Chemistry – A European Journal* **23** 3184-90
27 [16] Zhao M T, Deng K, He L C, Liu Y, Li G D, Zhao H J and Tang Z Y 2014 Core-Shell Palladium
28 Nanoparticle@Metal-Organic Frameworks as Multifunctional Catalysts for Cascade Reactions *J Am Chem
29 Soc* **136** 1738-41
30 [17] Hu P, Morabito J V and Tsung C K 2014 Core-Shell Catalysts of Metal Nanoparticle Core and Metal-Organic
31 Framework Shell *ACS Catal* **4** 4409-19
32 [18] Gao S T, Liu W H, Shang N Z, Feng C, Wu Q H, Wang Z and Wang C 2014 Integration of a plasmonic
33 semiconductor with a metal-organic framework: a case of Ag/AgCl@ZIF-8 with enhanced visible light
34 photocatalytic activity *RSC Adv* **4** 61736-42
35 [19] Li Y T, Tang J L, He L C, Liu Y, Liu Y L, Chen C Y and Tang Z Y 2015 Core-Shell Upconversion
36 Nanoparticle@Metal-Organic Framework Nanoprobes for Luminescent/Magnetic Dual-Mode Targeted
37 Imaging *Adv Mater* **27** 4075-80
38 [20] Kreno L E, Greenelch N G, Farha O K, Hupp J T and Van Duyne R P 2014 SERS of molecules that do not
39 adsorb on Ag surfaces: a metal-organic framework-based functionalization strategy *Analyst* **139** 4073-80
40 [21] He L, Liu Y, Liu J, Xiong Y, Zheng J, Liu Y and Tang Z 2013 Core-Shell Noble-Metal@Metal-Organic-
41 Framework Nanoparticles with Highly Selective Sensing Property *Angewandte Chemie International
42 Edition* **52** 3741-5
43 [22] Sugikawa K, Nagata S, Furukawa Y, Kokado K and Sada K 2013 Stable and Functional Gold Nanorod
44 Composites with a Metal-Organic Framework Crystalline Shell *Chem Mater* **25** 2565-70
45 [23] Houk R J T, Jacobs B W, El Gabaly F, Chang N N, Talin A A, Graham D D, House S D, Robertson I M and
46 Allendorf M D 2009 Silver Cluster Formation, Dynamics, and Chemistry in Metal-Organic Frameworks
47 *Nano Lett* **9** 3413-8
48 [24] Hu Y L, Liao J, Wang D M and Li G K 2014 Fabrication of Gold Nanoparticle-Embedded Metal-Organic
49 Framework for Highly Sensitive Surface-Enhanced Raman Scattering Detection *Anal Chem* **86** 3955-63

1 [25] Yu T H, Ho C H, Wu C Y, Chien C H, Lin C H and Lee S 2013 Metal-organic frameworks: a novel SERS
2 substrate *J Raman Spectrosc* **44** 1506-11
3 [26] Sugikawa K, Furukawa Y and Sada K 2011 SERS-Active Metal-Organic Frameworks Embedding Gold
4 Nanorods *Chem Mater* **23** 3132-4
5 [27] Zhao Y B, Kornienko N, Liu Z, Zhu C H, Asahina S, Kuo T R, Bao W, Xie C L, Hexemer A, Terasaki O, Yang P D
6 and Yaghi O M 2015 Mesoscopic Constructs of Ordered and Oriented Metal-Organic Frameworks on
7 Plasmonic Silver Nanocrystals *J Am Chem Soc* **137** 2199-202
8 [28] Ren F H, Wang X G, Li Z A, Luo J D, Jang S H, Jen A K Y and Wang A X 2014 Enhanced third harmonic
9 generation by organic materials on high-Q plasmonic photonic crystals *Opt Express* **22** 20292-7
10 [29] Kreno L E, Hupp J T and Van Duyne R P 2010 Metal-Organic Framework Thin Film for Enhanced Localized
11 Surface Plasmon Resonance Gas Sensing *Anal Chem* **82** 8042-6
12 [30] Ren F H, Kim K Y, Chong X Y and Wang A X 2015 Effect of finite metallic grating size on Rayleigh anomaly-
13 surface plasmon polariton resonances *Opt Express* **23** 28868-73
14 [31] Moharam M G and Gaylord T K 1981 Rigorous Coupled-Wave Analysis of Planar-Grating Diffraction *J Opt
15 Soc Am* **71** 811-8
16 [32] Steele J M, Moran C E, Lee A, Aguirre C M and Halas N J 2003 Metallodielectric gratings with
17 subwavelength slots: Optical properties *Phys Rev B* **68**
18 [33] Gao H, McMahon J M, Lee M H, Henzie J, Gray S K, Schatz G C and Odom T W 2009 Rayleigh anomaly-
19 surface plasmon polariton resonances in palladium and gold subwavelength hole arrays *Opt Express* **17**
20 2334-40
21 [34] Tian F Y, Mosier A M, Park A, Webster E R, Cerro A M, Shine R S and Benz L 2015 In Situ Measurement of
22 CO₂ and H₂O Adsorption by ZIF-8 Films *J Phys Chem C* **119** 15248-53

23
24
25
26
27
28
29
30
31
32
33
34
35
36
37
38
39
40
41
42
43
44
45
46
47
48
49
50
51
52
53
54
55
56
57
58
59
60